ACS APPLIED MATERIALS & INTERFACES

Letter

www.acsami.org

Coplanar Induction Enabled by Asymmetric Permittivity of Dielectric Materials for Mechanical Energy Conversion

Xue Jiao Zhao,[†] Guang Zhu,*[,†] and Zhong Lin Wang[†,‡]

[†]Beijing Institute of Nanoenergy and Nanosystems, Chinese Academy of Sciences, Beijing 100083, China

[‡]School of Materials Science and Engineering, Georgia Institute of Technology, Atlanta, Georgia 30332, United States

Supporting Information

ABSTRACT: Triboelectric nanogenerator (TENG) is a newly emerged technology for harvesting mechanical energy, which has the promise for various practical applications. Here, we introduce a new principle of TENG in which induced current is generated between two coplanar electrodes because of different dielectric fillers of distinct permittivities. The manipulation of permittivity of dielectric materials for TENG is first reported, demonstrating a novel route in designing high-performance TENGs. When repeatedly contacting with an object, a TENG having lateral dimensions of 21 mm × 10 mm can produce an open-circuit voltage of 58.5 V and a short-circuit current of 44.7 μA. The instantaneous output power density can reach up to 708 μW. Besides, the new design incorporates all electrodes into a single plane, greatly simplifying the structure, promoting robustness, and providing a viable solution for device miniaturization.

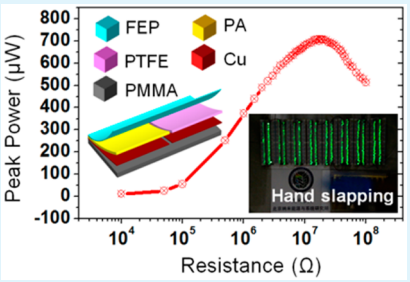

KEYWORDS: *energy conversion, triboelectric effect, relative permittivity, electrostatic induction*

Mechanical energy, because of its abundance and wide availability, is an ideal source for energy conversion and energy harvesting that extracts electric energy from ambient environment.[1−8] It provides an important route in obtaining cost-effective, clean, and sustainable electric power not only for small electronics but also for possibly large-scale power generation. Recently, triboelectric nanogenerator (TENG) as a new class of energy-harvesting technique was developed and has attracted increasingly extensive attentions.[9−13] Basically, once two thin films of distinct materials are in physical contact, net surface charges will transfer because of the different triboelectric polarities of the materials.[12−14] When the two films have relative motions that are either perpendicular or parallel to the planar films, induced charges flow between two separate electrodes that are on the back of each thin-film material. As a result, the two electrodes have to be in relative motion constantly, which poses several major problems for practical use of the device. First, the electronic packaging becomes susceptible to breakage that leads to device failure. Second, it takes extra room to incorporate the mobile electrodes into an enclosed structure, which makes it challenging for device miniaturization. Here, we introduce a new operating principle of the TENG in which induced current is generated between two coplanar electrodes attached to different dielectric filling layers with distinct permittivities. When repeatedly contacting with a separate object, a TENG having lateral dimensions of 21 mm × 10 mm can produce an open-circuit voltage of 58.5 V and a short-circuit current of 44.7 μA, corresponding to a peak power density of 708 μW. This new principle enables stationary electrodes on the same plane, which completely solves the aforementioned packaging problem. More importantly, the manipulation of permittivity of dielectric materials for TENG is first reported, demonstrating a novel route in designing high-performance triboelectric energy harvesters by tuning bulk properties of materials.

FABRICATION OF THE DEVICE

The asymmetric dielectric triboelectric nanogenerator (AD-TENG) has a multilayered structure, as sketched in Figure 1a. The top contact surface is made of fluorinated ethylene propylene (FEP) that is 10 μm in thickness. Beneath the top layer, the filling layer is composed of two adjacent dielectric

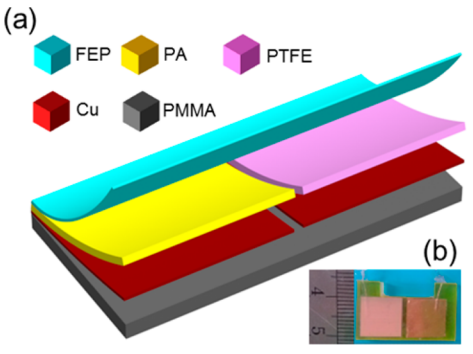

Figure 1. Structure of the AD-TENG. (a) Schematic diagram of an AD-TENG. (b) Photograph of the as-fabricated device.

Received: January 2, 2015
Accepted: March 3, 2015
Published: March 3, 2015

DOI: 10.1021/acsami.5b00019
ACS Appl. Mater. Interfaces 2015, 7, 6025−6029

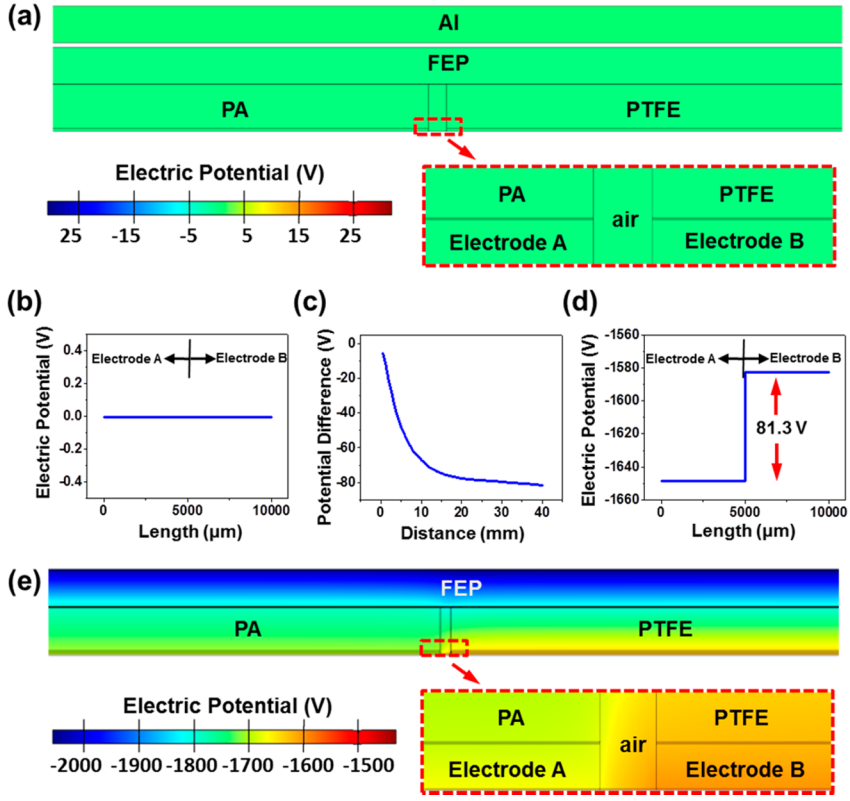

Figure 2. Simulation results of electric potential distributions by finite-element method. (a) Electric potential distribution in the contact state. Inset: enlarged view of the electric potential distribution on the two electrodes. (b) Electric potential distribution on the two electrodes across the length of the device in the contact state. (c) Simulated result of the open-circuit voltage as the contact leaves away from the device. (d) Electric potential distribution on the two electrodes across the length of the device in the separation state (e) Electric potential distribution in the separation state. Inset: enlarged view of the electric potential distribution on the two electrodes.

materials of the same dimensions (30 μm in thickness) but different permittivities. Polyamide (PA) at one side has a higher relative permittivity than that of polytetrafluoroethylene (PTFE) at the other side. Each dielectric material has a copper back electrode of 200 nm made by electron beam deposition. For easy reference, the one under the PA is denoted as the electrode A; and the one beneath the PTFE film is referred to as the electrode B. They are connected to the positive and negative terminals of an electrometer for electrical measurement, respectively. The multilayered structure is adhered onto an acrylic substrate of 1 mm in thickness. The entire device has lateral dimensions of 21 mm × 10 mm, while each electrode is square-shaped with a side length of 10 mm.

■ ANALYTICAL MODE

The energy generation of the AD-TENG relies on reciprocating motion between the device and an external object made of a material other than FEP. To illustrate this process, we selected two special states. One is the contact state in which the top surface of the device and the object are in complete contact; the other is the separation state in which the object is far apart from the device. The open-circuit voltage of the AD-TENG is defined by the following eq 1

$$V_{oc} = \varphi_A - \varphi_B \quad (1)$$

where φ_A and φ_B are the electric potentials of the electrodes A and B, respectively. In the contact state, equal and opposite triboelectric charges are generated on the contact surfaces. Due to strong electron affinity of fluorine, the FEP surface is always

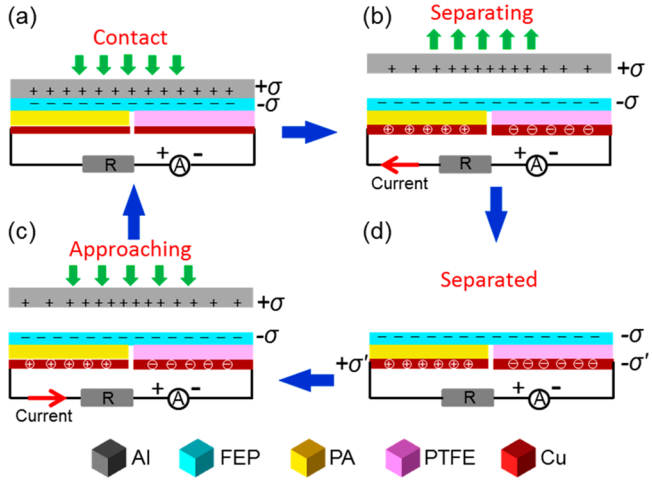

Figure 3. Sketches that illustrate the electricity-generation process of the AD-TENG. (a) The contact state does not induce unbalanced charges on the two electrodes. (b) As the object separates apart, induced current flows from the electrode B to the electrode A. (c) As the object approaches the AD-TENG, induced current flows back from the electrode A to the electrode B. (d) Maximum induced charges are generated in the separation state.

negatively charged as a result of contact electrification,[15−17] leaving the object surface positively charged. Because the surface charges are completely canceled out by their opposite counterparts in the contact state, the open-circuit voltage is zero. If the object moves away, the negative triboelectric charges left on the

DOI: 10.1021/acsami.5b00019
ACS Appl. Mater. Interfaces 2015, 7, 6025−6029

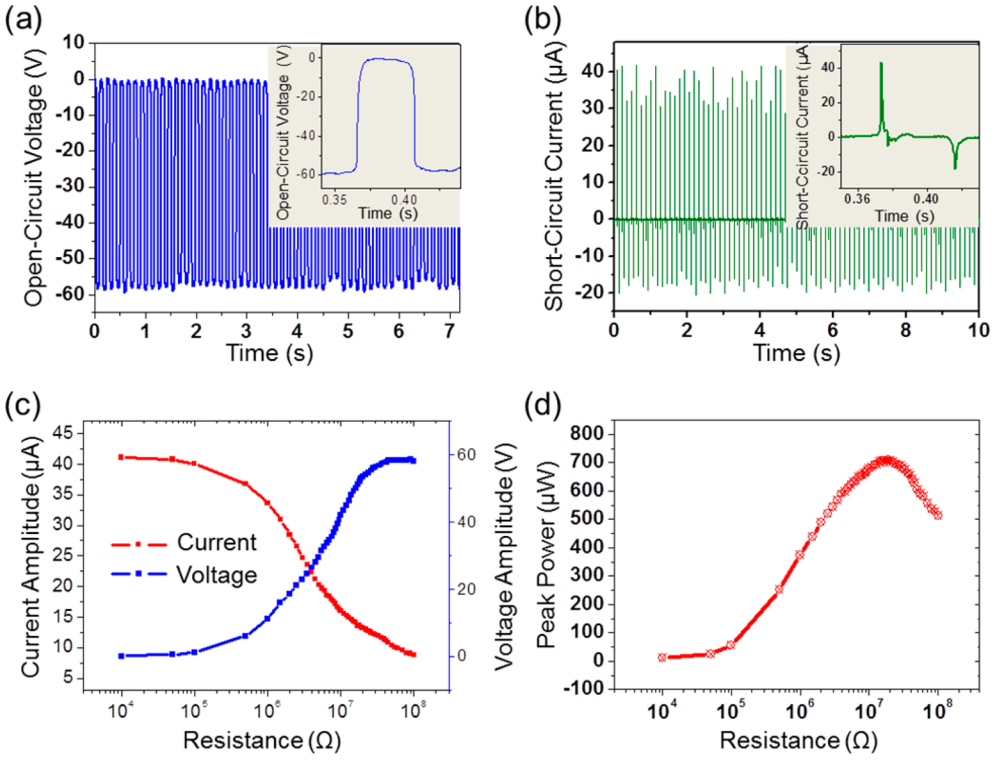

Figure 4. Electric output characteristics of an AD-TENG when triggered by external mechanical impact. (a) Open-circuit voltage and (b) short-circuit current of the AD-TENG. Insets: enlarged views of a single cycle. (c) Dependence of the output voltage and output current amplitude as a function of the circuit load resistance. (d) Peak output power of the AD-TENG as a function of the circuit load resistance.

FEP surface produce asymmetric electric potential between the two electrodes. As described in eq 2 below, the output voltage in the separation state is

$$V_{oc} = \left(\frac{\sigma d}{2\varepsilon_0\varepsilon_{PA}} + \frac{\sigma d_{FEP}}{2\varepsilon_0\varepsilon_{FEP}}\right) - \left(\frac{\sigma d}{2\varepsilon_0\varepsilon_{PTFE}} + \frac{\sigma d_{FEP}}{2\varepsilon_0\varepsilon_{FEP}}\right) = \frac{\sigma d}{2\varepsilon_0}\left(\frac{1}{\varepsilon_{PA}} - \frac{1}{\varepsilon_{PTFE}}\right) \quad (2)$$

where σ is the triboelectric charge density on the FEP surface; ε_0 is the vacuum permittivity; ε_{PA}, ε_{PTFE}, and ε_{FEP} are the relative permittivities of PA, PTFE, and FEP, respectively; d is thickness of the dielectric filling layer; and d_{FEP} is thickness of the top FEP. As indicated in the above equation, the origin of the open-circuit voltage lies in the asymmetric permittivities of the two dielectric materials.

In the work, the object made of aluminum is used because it can produce large triboelectric charge density after contacting with FEP.[16] By substituting specific values into eq 2 (σ =−2 × 10−4 C/m^2,[14,18] d = 30 μm, ε_{PTFE} = 2.0, ε_{PA} = 4.0), the maximum open-circuit voltage is calculated to be ∼85 V.

THEORETICAL SIMULATION VIA COMSOL

2D model that matches the actual profile of the device was built via COMSOL. Open-circuit condition was applied. The charge density on the FEP surface was assigned to be -2×10^{-4} C/m^2. The surface of the contact object was assigned a total surface charge of $Q = 4.2 \times 10^{-8}$ C ($Q = \sigma s$, where s is the area of the FEP film). As shown in Figure 2a, b, the electric potential of the two electrodes is 0 in the contact state, which corresponds to no open-circuit voltage. As the aluminum object moves away from the top surface of the AD-TENG, the open-circuit voltage first linearly decreases and then drops at a slower rate until it saturates, as illustrated in Figure 2c. The saturation essentially corresponds to the separation state where the object is absent. The saturated open-circuit voltage of −81.3 V is revealed in Figure 2d, e, which agrees well with that from the analytical calculation. It is to be noted that the open-circuit voltage is only dependent on the position of the object and can keep stable as long as the object remains stationary.

ELECTRICITY GENERATION PROCESS

To illustrate how the electricity is generated, we connected the two electrodes so that free electrons can redistribute between them because of electrostatic induction. In the contact state, there is no induced charge on either of the electrodes because of the balanced electric potential (Figure 3a). As the aluminum object leaves, negative charges on the FEP surface will alter the electric potential on the back electrodes because of leakage of electric field. Then the electrode B tends to have a higher electric potential than the electrode A because of the higher permittivity on the PA side. As a result, free electrons flow from the electrode A to electrode B in order to screen the electric potential difference, resulting in positive induced charges on the electrode A and negative ones on the electrode B. As a result, a negative current can be measured (Figure 3b) until the separation state is reached (Figure 3d). When the positively charged object approaches the device, induced charges redistribute and flow back in the opposite direction, producing a positive current (Figure 3c) until the contact state is restored (Figure 3a). Therefore, as the object makes reciprocating motion with respect to the device, electrons or induced charges are pumped back and forth between the two electrodes, producing alternating current and thus realizing the conversion of mechanical energy.

DOI: 10.1021/acsami.5b00019
ACS Appl. Mater. Interfaces 2015, 7, 6025−6029

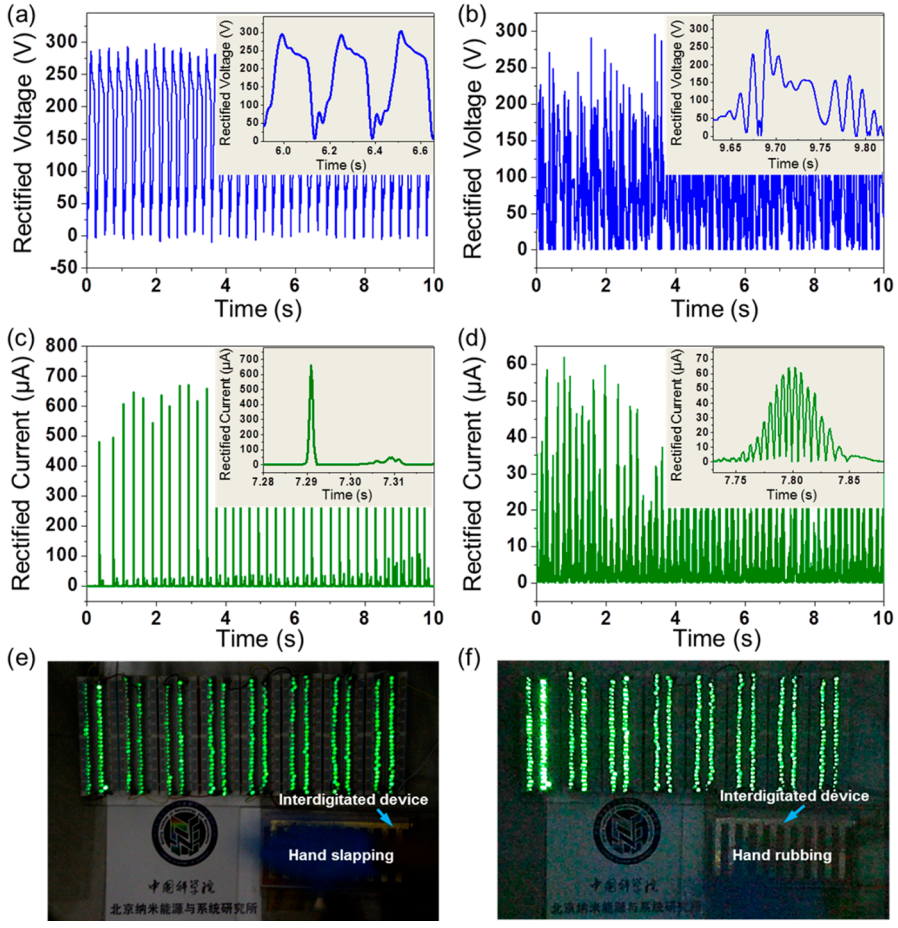

Figure 5. Application demonstrations of an area-scalable AD-TENG with an interdigitated structure. Rectified voltage of the interdigitated AD-TENG when (a) slapped and (b) rubbed by a gloved hand (Insets: enlarged views). Rectified current of the interdigitated AD-TENG when slapped (c) and rubbed (d) by a gloved hand (Insets: enlarged views). Picture of LEDs powered by the interdigitated AD-TENG (e) slapped and (f) rubbed by a gloved hand.

In this work, an AD-TENG was mechanically triggered by an electromagnetic vibration exciter that provides dynamic impact with controlled force at a frequency of 9 Hz. The short-circuit current and open-circuit voltage were measured separately to characterize the electric performance of the device. The open-circuit voltage switches between zero and a maximum value of 58.5 V, which correspond to the contact and separation states, respectively (Figure 4a). The amplitude of the alternating short-circuit current reaches up to 44.7 μA (Figure 4b). The positive and negative current peaks correspond to the approaching and separating processes in Figure 3, respectively. It is observed that positive peaks are higher but narrower than the negative ones although they carry the same amount of induced charges (inset in Figure 4b). Such an observation can be explained by the fact that the separating process is faster. The measured electric output coincides with that obtained from the above theoretical analysis, which further validates the proposed operating principle. To investigate the actual output power of the AD-TENG, we obtained load matching curves using an external load resistor varying from 0.1 MΩ to 100 MΩ, as shown in Figure 4c, d. As the resistance increases, the current amplitude decreases, while the voltage amplitude rises. Consequently, the instantaneous power that is delivered onto the load by the device exhibits a maximum value of 708 μW at the optimum load resistance of 19 MΩ (Figure 4d). It corresponds to an area power density of 337 μW/cm^2.

To demonstrate the potential applications of the AD-TENG, we fabricated an enlarged device having lateral dimensions of 200 mm by 90 mm. It has a planar interdigitated structure (Figure 1 in the Supporting Information). Each tooth has a width of 10 mm and length of 69 mm; and the interval between adjacent teeth is 1 mm. When the device was slapped by a gloved hand at a speed of about 3 m/s, it generated an open-circuit voltage and a rectified short-circuit current of 300 V (Figure 5a) and 0.7 mA (Figure 5c), respectively. 500 LED bulbs were lighted up (Figure 5e, movie in the Supporting Information). Moreover, when the hand was rubbing against the device at a speed of 0.2 m/s without separation, an open-circuit voltage of 300 V (Figure 5b) and a rectified short-circuit current of 60 μA (Figure 5d) were also generated, which could still power the LED arrays (Figure 5f, movie in the Supporting Information). It is noticed that the voltage output has similar amplitude for the two kinds of motions while the current amplitude has significant difference. This is because the voltage output is independent of the motion speed; but the current output is directly related to the motion speed. Because the hand slapping is much faster than the hand rubbing, the current amplitude in Figure 5c is considerably higher than that in Figure 5d. These demonstrations reveal the capability of the AD-TENG in harnessing multiple types of mechanical motions because of its unique structural design.

DOI: 10.1021/acsami.5b00019
ACS Appl. Mater. Interfaces 2015, 7, 6025−6029

In summary, we developed a new approach of an AD-TENG for harvesting ambient mechanical energy of multiple types. With an effective contact area of 21 mm × 10 mm, the open-circuit voltage is up to 58.5 V and the short-circuit current amplitude reaches to 44.7 μA, corresponding to a peak power density of 708 μW. As this new principle enables stationary electrodes, the basic concept and design in this work demonstrate a novel route in designing triboelectric energy harvesters and can be extended to other configurations that are applicable to harvest multiple forms of ambient mechanical energy.

■ ASSOCIATED CONTENT

Supporting Information

A schematic illustrating the interdigitated structure of an enlarged AG-TENG; a movie that shows powering LED arrays by the enlarged AG-TENG when it is triggered by hand slapping and hand rubbing. This material is available free of charge via the Internet at http://pubs.acs.org.

■ AUTHOR INFORMATION

Corresponding Author

*E-mail: zhuguang@binn.cas.cn.

Notes

The authors declare no competing financial interest.

■ ACKNOWLEDGMENTS

The research was supported by the "thousands talents" program for pioneer researcher and his innovation team, China, Beijing City Committee of science and technology project (Z131100006013004). Patents have been filed based on the research presented here.

■ REFERENCES

(1) Wang, X.; Song, J.; Liu, J.; Wang, Z. L. Direct-Current Nanogenerator Driven by Ultrasonic Waves. *Science* **2007**, *316*, 102−107.

(2) Kuo, A. D. Biophysics. Harvesting Energy by Improving the Economy of Human Walking. *Science* **2005**, *309*, 1686−1693.

(3) Jeong, C. K.; Baek, K. M.; Niu, S.; Nam, T. W.; Hur, Y. H.; Park, D. Y.; Hwang, G.-T.; Byun, M.; Wang, Z. L.; Jung, Y. S.; Lee, K. J. Topographically-Designed Triboelectric Nanogenerator via Block Copolymer Self-Assembly. *Nano Lett.* **2014**, *14*, 7031−7038.

(4) Meng, X. S.; Zhu, G.; Wang, Z. L. Robust Thin-Film Generator Based on Segmented Contact-Electrification for Harvesting Wind Energy. *ACS Appl. Mater. Interfaces* **2014**, *6*, 8011−8017.

(5) Ma, M.; Guo, L.; Anderson, D. G.; Langer, R. Bio-Inspired Polymer Composite Actuator and Generator Driven by Water Gradients. *Science* **2013**, *339*, 186−195.

(6) Krupenkin, T.; Taylor, J. A. Reverse Electrowetting as A New Approach to High-Power Energy Harvesting. *Nat. Commun.* **2011**, *2*, 448−456.

(7) Dagdeviren, C.; Yang, B. D.; Su, Y.; Tran, P. L.; Joe, P.; Anderson, E.; Xia, J.; Doraiswamy, V.; Dehdashti, B.; Feng, X.; Lu, B.; Poston, R.; Khalpey, Z.; Ghaffari, R.; Huang, Y.; Slepian, M. J.; Rogers, J. A. Conformal Piezoelectric Energy Harvesting and Storage from Motions of the Heart, Lung, and Diaphragm. *Proc. Natl. Acad. Sci. U.S.A.* **2014**, *5*, 1927−1932.

(8) Guigon, R.; Chaillout, J.-J.; Jager, T.; Despesse, G. Harvesting Raindrop Energy: Experimental Study. *Smart Mater. Struct.* **2008**, *17*, 015039−015046.

(9) Fan, F.-R.; Tian, Z.-Q.; Lin Wang, Z. Flexible Triboelectric Generator. *Nano Energy* **2012**, *1*, 328−334.

(10) Wang, Z. L. Triboelectric Nanogenerators as New Energy Technology for Self-Powered Systems and as Active Mechanical and Chemical Sensors. *ACS Nano* **2013**, *7*, 9533−9557.

(11) Leng, Q.; Guo, H.; He, X.; Liu, G.; Kang, Y.; Hu, C.; Xi, Y. Flexible Interdigital-Electrodes-Based Triboelectric Generators for Harvesting Sliding and Rotating Mechanical Energy. *J. Mater. Chem. A* **2014**, *2*, 19427−19434.

(12) Su, Y.; Yang, Y.; Zhong, X.; Zhang, H.; Wu, Z.; Jiang, Y.; Wang, Z. L. Fully Enclosed Cylindrical Single-Electrode-based Triboelectric Nanogenerator. *ACS appl. Mater. Interfaces* **2014**, *6*, 553−559.

(13) Zhang, X.-S.; Han, M.-D.; Wang, R.-X.; Zhu, F.-Y.; Li, Z.-H.; Wang, W.; Zhang, H.-X. Frequency-Multiplication High-Output Triboelectric Nanogenerator for Sustainably Powering Biomedical Microsystems. *Nano Lett.* **2013**, *13*, 1168−1172.

(14) Zhu, G.; Chen, J.; Zhang, T.; Jing, Q.; Wang, Z. L. Radial-Arrayed Rotary Electrification for High Performance Triboelectric Generator. *Nat. Commun.* **2014**, *5*, 3426−3431.

(15) Wiles, J. A.; Grzybowski, B. A.; Winkleman, A.; Whitesides, G. M. A Tool for Studying Contact Electrification in Systems Comprising Metals and Insulating Polymers. *Anal. Chem.* **2003**, *75*, 4859−4867.

(16) Diaz, A. F.; Felix-Navarro, R. M. A Semi-Quantitative Triboelectric Series for Polymeric Materials: the Influence of Chemical Structure and Properties. *J. Electrostat.* **2004**, *62*, 277−290.

(17) Panat, R.; Jinlin, W.; Parks, E. Effects of Triboelectrostatic Charging between Polymer Surfaces in Manufacturing and Test of Integrated Circuit. *IEEE Trans. Compon., Packag., Manuf. Technol.* **2014**, *4*, 943−946.

(18) Chen, J.; Zhu, G.; Yang, W.; Jing, Q.; Bai, P.; Yang, Y.; Hou, T. C.; Wang, Z. L. Harmonic-Resonator-Based Triboelectric Nanogenerator as a Sustainable Power Source and a Self-Powered Active Vibration Sensor. *Adv. Mater.* **2013**, *25*, 6094−6099.

DOI: 10.1021/acsami.5b00019
ACS Appl. Mater. Interfaces 2015, 7, 6025−6029